Research paper

Chaos synchronization in generalized Lorenz systems and an application to image encryption

Sungju Moon [a], Jong-Jin Baik [a,*], Jaemyeong Mango Seo [b]

[a] *School of Earth and Environmental Sciences, Seoul National University, Seoul 08826, South Korea*
[b] *Max Planck Institute for Meteorology, Bundesstraße 53, Hamburg 20146, Germany*

ARTICLE INFO

ABSTRACT

Examples of synchronization, pervasive throughout the natural world, are often awe-inspiring because they tend to transcend our intuition. Synchronization in chaotic dynamical systems, of which the Lorenz system is a quintessential example, is even more surprising because the very defining features of chaos include sensitive dependence on initial conditions. It is worth pursuing, then, the question of whether high-dimensional extensions of such a system also exhibit synchronization. This study investigates synchronization in a set of high-dimensional generalizations of the Lorenz system obtained from the inclusion of additional Fourier modes. Numerical evidence supports that these systems exhibit self-synchronization. An example application of this phenomenon to image encryption is also provided. Numerical experiments also suggest that there is much more to synchronization in these generalized Lorenz systems than self-synchronization; while setting the dimension of the driver system higher than that of the receiver system does not result in perfect synchrony, the smaller the dimensional difference between the two, the more closely the receiver system tends to follow the driver, leading to self-synchronization when their dimensions are equal.

© 2021 The Authors. Published by Elsevier B.V.
This is an open access article under the CC BY-NC-ND license
(http://creativecommons.org/licenses/by-nc-nd/4.0/)

1. Introduction

The Lorenz system [1] is a popular example of a relatively simple deterministic system exhibiting chaos. In the midst of chaos, however, there stands a curious and seemingly contradictory emergence of order when two chaotic systems are coupled in a specific manner. Chaos synchronization occurs when two coupled chaotic dynamical systems ultimately yield identical or synchronized solutions regardless of their initial conditions. The coupling can take many different forms. For example, under unidirectional coupling, one system, called the driver, transmits limited information about its solutions to the other system, called the receiver, but not the other way around. When both the driver and the receiver are assigned identical systems, the resulting synchronization under such a set-up is referred to as *self-synchronization*, which the Lorenz system is known to exhibit [2,3]. The discovery of chaos synchronization was soon followed by promising developments of various applications in different disciplines including population dynamics [4], climatology [5], data assimilation [6], and secure communication technologies [7].

---

* Corresponding author
  E-mail address: jjbaik@snu.ac.kr (J.-J. Baik).

One of the questions raised early on was whether self-synchronization might also be possible in hyperchaotic systems in higher dimensions, which was quickly answered in the affirmative [8,9]. There has recently been a resurgence of interest in high-dimensional extensions of the Lorenz and Lorenz-like systems [10–14], some exploring the possibility of finding hyperchaos [15,16]. One way to raise the dimension of the Lorenz system is by including additional modes when truncating the Fourier series in the derivation. Done consistently, these extensions are akin to considering smaller-scale motions in the thermal convection model, bringing the Lorenz system closer to the original governing equations, a version of the Navier-Stokes equations. It has recently been noted in [17] that this way of raising the dimension leads to $(3N)$- and $(3N+2)$-dimensional generalizations of the Lorenz system for any positive integer N, which the present study aims to investigate for chaos synchronization.

There are two main advantages of using the aforementioned $(3N)$- and $(3N+2)$-dimensional generalizations to study chaos synchronization. First, being able to set N to be any positive integer, one can study whether self-synchronization is a dimension-invariant property of this family of generalized Lorenz systems. Second, by experimentally assigning the driver and receiver systems with different dimensions, one can investigate whether there occurs synchronization in a more general sense beyond self-synchronization. One interesting aspect about this set-up is that the driver and receiver systems, though not identical, still belong to the same family of systems. The possibility of synchronization between high- and low-dimensional systems in this way has a particularly important conceptual link with modeling studies because any dynamical model for a natural phenomenon is likely a smaller subset of the actual system that governs the phenomenon [6]. From this perspective, a model may not accurately simulate the reality unless there is synchronization between the reality, a higher-dimensional system, and the model, a lower-dimensional system.

Motivated by these advantages, both from the theoretical and modeling perspectives, the first goal of this study is to present convincing numerical evidence in support of self-synchronization in these systems, requiring only the transmission of the same amount of information sufficient for guaranteeing self-synchronization in the original three-dimensional Lorenz system. It is demonstrated that this unique feature of the generalized systems allows for a potentially useful application in chaos-based image encryption. The second goal of this study is to identify, if any, an indication of generalized synchronization between two Lorenz systems differing in their dimensions. This has led to the identification of a surprising pattern relating generalized synchronization with dimensionality, hinting at a generalizing principle that may encompass self-synchronization as its special case.

Section 2 briefly introduces the generalized Lorenz systems. Self-synchronization in these systems is discussed in Section 3 followed by a simple demonstration of an application to image encryption (Section 4). Section 5 explores generalized synchronization between two systems with different dimensions. A summary and conclusions are given in Section 6.

2. Equations

The three-dimensional Lorenz system [1] consists of the following three ordinary differential equations in three variables, X, Y, and Z:

$$\dot{X} = -\sigma X + \sigma Y, \tag{1}$$

$$\dot{Y} = rX - Y - XZ, \tag{2}$$

$$\dot{Z} = -bZ + XY, \tag{3}$$

where r is the Rayleigh parameter, σ is the Prandtl number, and b is a geometric parameter. The dot above each variable indicates its first derivative with respect to time t. In [17], the three variables, X, Y, and Z are generalized as the kth variables, X_k, Y_k, and Z_k, respectively, leading to a system with either $(3N)$ or $(3N+2)$ ordinary differential equations, where N is the number of equations with $\dot{X}_k$ on the left-hand-side. Typically, the derivations of Lorenz systems based on the governing equations for Rayleigh-Bénard convection involve truncating Fourier series expansions [11]. Accordingly, these $(3N)$- and $(3N+2)$-dimensional systems are generalizations of the ordinary differential equation systems obtained by choosing different numbers of modes to survive the truncation [17]. Although $(3N+1)$-dimensional systems appear to be missing from these generalizations, as explained in [18], attempting to derive a $(3N+1)$-dimensional system results in some extraneous sinusoidal terms with which any such purported system of $(3N+1)$ ordinary differential equations would not be reduced to the Lorenz system, and thus they are not included in the generalization.

The $(3N)$-dimensional system is given by the following equations for each positive integer $k \leq N$:

$$\dot{X}_k = -d_k \sigma X_k + \frac{\sigma}{d_k} Y_k, \tag{4}$$

$$\dot{Y}_k = rX_k - d_k Y_k + \sum_{(i,j) \in P_k} \left(jX_i Z_j \mathscr{S}_Y \right), \tag{5}$$

$$\dot{Z}_k = -k^2 b Z_k + \sum_{(i,j)\in Q_k} \left(k X_i Y_j \mathscr{S}_Z \right), \tag{6}$$

where i and j are indices that form integer pairs belonging to the set P_k or the set Q_k defined for each k. These sets P_k and Q_k are given by

$$P_k = \{(i,j) : i+j = k\} \cup \{(i,j) : j-i = k-1\} \cup \{(i,j) : i-j = k\}, \tag{7}$$

$$Q_k = \{(i,j) : |j-i| = k\} \cup \{(i,j) : j+i = k+1\}. \tag{8}$$

The sign functions $\mathscr{S}_Y$ and $\mathscr{S}_Z$ depend on which of the conditions in the above definitions of P_k and Q_k are satisfied: $\mathscr{S}_Y = -1$ if $j - i = k - 1$ and $\mathscr{S}_Y = 1$ if otherwise and $\mathscr{S}_Z = -1$ if $|j - i| = k$ and $\mathscr{S}_Z = 1$ if otherwise. Here, $d_k = (a^2 + (2k-1)^2)/(1 + a^2)$, where a is usually set as $1/\sqrt{2}$.

The $(3N + 2)$-dimensional system is comprised of N number of X variables and $N + 1$ number of Y and Z variables each. The first $3N$ equations are also given by Eqs. (4)–(6), but note that i and j can now go up to $N + 1$. The additional equations for $k = N + 1$ are given by

$$\dot{Y}_k = -d_k Y_k + \sum_{(i,j)\in P_k} \left(j X_i Z_j \mathscr{S}_Y \right), \tag{9}$$

$$\dot{Z}_k = -k^2 b Z_k + \sum_{(i,j)\in Q_k} \left(k X_i Y_j \mathscr{S}_Z \right). \tag{10}$$

Detailed derivations of these $(3N)$- and $(3N + 2)$-dimensional generalizations of the Lorenz system are found in [17], which also contains periodicity diagrams for these systems in various parameter spaces. Such periodicity diagrams provide information pertaining to which parameter pairs are likely to yield chaotic solutions. Given the standard value for $b = 8/3$, the parameter values around $r \sim 500$ and $\sigma \sim 50$ are reliable choices for harnessing chaos from these systems up to dimension ~ 33. For this reason, in this study these parameter values are used extensively for numerically testing the generalized Lorenz systems for chaos synchronization.

3. Self-synchronization

3.1. Numerical evidence

To test for self-synchronization, the driver and receiver systems are assigned the same dimensions with only the solutions to variable X_1 being sent from the driver to the receiver. More precisely, suppose the driver and receiver are both assigned the $(N + M)$-dimensional generalized Lorenz systems consisting of the ordinary differential equations of the form (4)–(6) if $N = M$ and also (9)–(10) if $M = N + 1$. Denote the driver system's solution at time t by $\mathbf{X}_D(t) = (X_{1,D}, \dots, X_{N,D}, Y_{1,D}, \dots, Y_{M,D}, Z_{1,D}, \dots, Z_{M,D})$. Likewise, denote the receiver system's solution at time t by $\mathbf{X}_R(t)$. The computation of their numerical solutions is done using the fourth-order Runge-Kutta method with the time step size $\Delta t = 10^{-4}$. If the receiver system's solution for X_1 is replaced by $X_{1,D}$ at every time step before the solution is fed back into the differential equation solver, the driver is said to *transmit* to the receiver the variable X_1. The $(N + M)$-dimensional system can be said to self-synchronize under the transmission of X_1 if the driver transmitting X_1 implies $\lim_{t\to\infty} (\mathbf{X}_D(t) - \mathbf{X}_R(t)) = \mathbf{0}$; however, in most cases where a Lorenz system does self-synchronize, we have found that this convergence between the numerical solutions happens rather quickly, making it feasible to check numerically in finite time.

In Fig. 1, all three systems with dimensions 3, 12, and 30 appear to exhibit self-synchronization under the transmission of variable X_1. Note that self-synchronization in the three-dimensional Lorenz system is already known. A mathematical proof of self-synchronization can be established if an appropriate Lyapunov function for the error subsystem is found, which has been done for the three-dimensional Lorenz system [19]. This appears to be a challenging problem for the high-dimensional Lorenz systems with dimension ≥ 6, let alone for the $(3N)$- and $(3N + 2)$-dimensional generalizations. A common strategy to finding a Lyapunov function, also adopted by Cuomo and Oppenheim [7], is cleverly pairing up the equations in the error subsystem so that the nonlinear terms would cancel out one another. There are two main difficulties in adopting such a strategy in our generalized systems. The first reason is in the increased complexity of the system. As the dimension gets higher, the P_k- and Q_k-sets increasingly contain a greater number of permutations for the (i,j)-pairs such that it quickly becomes infeasible to find the nonlinear terms with matching coefficients and opposite signs. In fact, the number of nonlinear pairs to be included follows a quasi-exponential curve [17]. The second reason has to do with the peculiar requirement that only X_1 is transmitted from the driver to the receiver. It can be seen in (4) that raising the dimension beyond dimension 6 introduces additional X_k variables. When X_1 is the only X variable in the system, finding a Lyapunov function comes down to a manipulation of the $\dot{Y}_k$ and $\dot{Z}_k$ equations in equal numbers, and so pairings follow naturally. On the other hand, each extra X_k whose driver solution is not made available to the receiver introduces additional complications to this strategy.
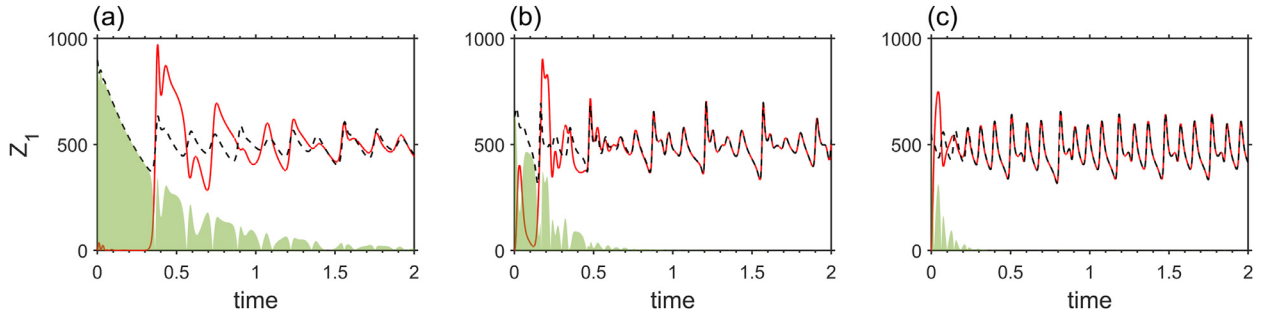
Fig. 1. Time series of the numerical solutions to Z_1 in the driver (black, dashed) and receiver (red, solid) systems of dimension (a) 3, (b) 12, and (c) 30 with $r = 500$, $\sigma = 50$, and $b = 8/3$, each starting at a different initial condition. The green shades indicate the absolute difference. (For interpretation of the references to color in all figure legends, the reader is referred to the web version of this article.)
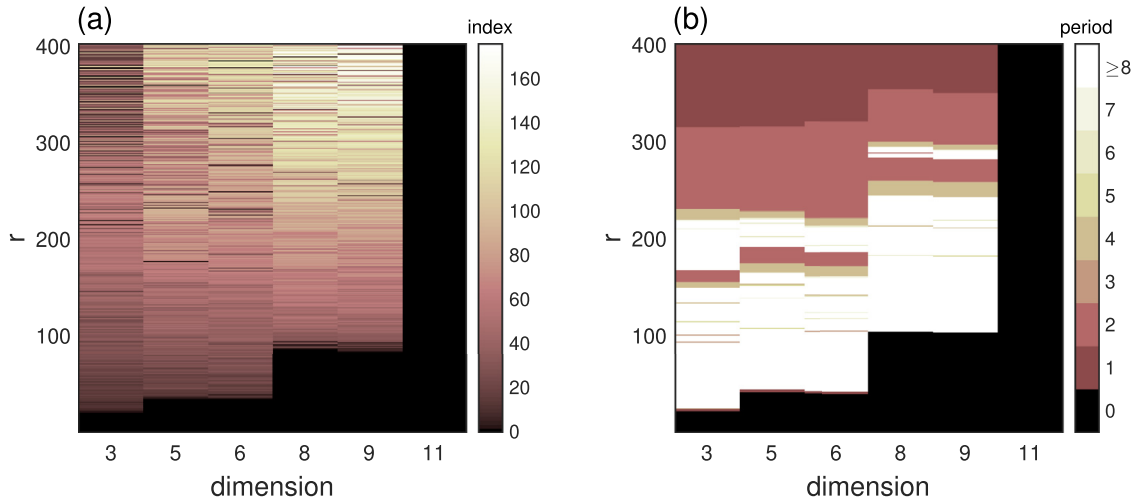

Fig. 2. Dimension-r space with $\sigma = 10$ and $b = 8/3$ showing (a) synchronization index γ computed with the initial condition $(X_1, Y_1, Z_1, \ldots) = (1, 0, 0, \ldots)$ given for the driver system and that with the perturbation of $+50$ added to Z_1 for the receiver and independent systems and (b) periodicity of the driver's solutions, a subset of results from Moon et al. [17].

Nevertheless, the numerical results indicate that the absolute differences between the driver's and receiver's solutions quickly approach 0 even in the relatively high-dimensional systems. Various different dimension and parameter combinations are further tested for self-synchronization, with more or less the equivalent results. In the particular cases shown in Fig. 1, the higher-dimensional systems even appear to self-synchronize more quickly than the three-dimensional system.

For a quantitative measure of self-synchronization, define the *synchronization index γ* based on root-mean-square differences (rmsd) as follows:

$$\gamma = \sqrt{\frac{1}{n} \sum_i \left(Z_{1,D}^{(i)} - Z_{1,I}^{(i)} \right)^2} - \sqrt{\frac{1}{n} \sum_i \left(Z_{1,D}^{(i)} - Z_{1,R}^{(i)} \right)^2}, \tag{11}$$

where subscripts D, R, and I stand for the driver system, the receiver system, and an independent system, respectively. The receiver system R is the system with the states of variable $X_1 = X_{1,R}$ replaced by the driver's solution to variable $X_1 = X_{1,D}$. While the independent system I is identical to the receiver system R in form and initial conditions, it does not receive the solutions $X_{1,D}$ from the driver and thus is independent of the driver system D. In Eq. (11), i and n are, respectively, the time step index and the number of time steps in the duration over which the rmsd are computed so that $Z_{1,D}^{(i)}$ denotes the solution to variable Z_1 in the driver system D at the ith time step. If self-synchronization occurs between D and R, then the rmsd between the driver's and receiver's solutions are expected to be smaller than those between the driver and independent solutions. Therefore, if $\gamma \gg 0$, it can be deduced that the detected synchronization is attributable to the coupling set-up. On the other hand, if $\gamma \leq 0$, then either there is no synchronization attributable to the coupling set-up or the two systems synchronize trivially; that is, they only appear to synchronize because both solutions are stable.

Fig. 2(a) shows the synchronization index in a dimension-r space with $\Delta r = 1$, computed from the numerical solutions in $t \in [50, 70]$ for each dimension-parameter combination. Note that the coupling and the perturbation to the initial condition are not made until after $t = 50$. Here, the driver system is given the initial condition $(X_1, Y_1, Z_1, \ldots) = (1, 0, 0, \ldots)$.

The receiver and independent systems are given the same initial conditions but with Z_1 perturbed by $+50$. The dimension-r periodicity diagram following the peak-counting scheme of [17] is plotted in Fig. 2(b) for reference, showing for which dimension-r pairs the solution is chaotic (period ≥ 8), periodic ($0 <$ period < 8), and stable (period $= 0$). Nowhere in the parameter-r space shown in Fig. 2(a), we have $\gamma < 0$. In fact, $\gamma \gg 0$ wherever there lies a non-stable solution. Observe also the abrupt transition from $\gamma > 0$ to $\gamma = 0$ at the demarcations between the areas of stable and non-stable solutions, implying that the convergence of stable solutions occurs within the initial spin-up time $t \in [0, 50]$ and therefore is distinguishable from convergence due to self-synchronization.

3.2. The error subsystems

Again, the complexity of the generalized Lorenz systems in Eqs. (4)–(10) makes finding appropriate Lyapunov functions of the error subsystems quite difficult, but the error subsystems can still be analyzed numerically.

First consider a simpler case in which the solutions to all X_k, $1 \leq k \leq N$, from the driver system are sent to the receiver system. This is a stronger condition than the conventional coupling set-up discussed so far, where only the solutions to X_1 are sent from the driver to the receiver system. Let δX_k, δY_k, and δZ_k denote the deviation of the receiver's variables from the driver's variables for each k by setting

$$Y_k' = Y_k + \delta Y_k, \tag{12}$$

$$Z_k' = Z_k + \delta Z_k, \tag{13}$$

where the prime indicates that the variable belongs to the receiver system. The error subsystem in δY_k and δZ_k is then given by

$$\frac{d}{dt}\delta Y_k = -d_k \delta Y_k + \sum_{(i,j) \in P_k} \left(j X_i \delta Z_j \mathscr{S}_Y \right), \tag{14}$$

$$\frac{d}{dt}\delta Z_k = -k^2 b \delta Z_k + \sum_{(i,j) \in Q_k} \left(k X_i \delta Y_j \mathscr{S}_Z \right), \tag{15}$$

for each positive integer $k \leq N$. The absence of r in the error subsystem comprised of Eqs. (14)–(15) strongly suggests that this system is stable, in which case the driver and receiver systems would self-synchronize.

Returning to the original condition for self-synchronization in question, suppose now only the solution to X_1 is transmitted from the driver to the receiver. Note that in this situation the receiver's variables corresponding to X_k for $k > 1$ must also be decomposed into $X_k' = X_k + \delta X_k$. We obtain the following error subsystem for the $(3N)$-dimensional cases:

$$\frac{d}{dt}\delta X_k = \begin{cases} 0 & \text{for } k = 1, \\ -d_k \sigma \delta X_k + \dfrac{\sigma}{d_k}\delta Y_k & \text{for } 2 \leq k \leq N, \end{cases} \tag{16}$$

and for each positive integer $k \leq N$,

$$\frac{d}{dt}\delta Y_k = r\delta X_k - d_k \delta Y_k + \sum_{(i,j) \in P_k} \left(j \left(X_i \delta Z_j + \delta X_i Z_j + \delta X_i \delta Z_j \right) \mathscr{S}_Y \right), \tag{17}$$

$$\frac{d}{dt}\delta Z_k = -k^2 b \delta Z_k + \sum_{(i,j) \in Q_k} \left(k \left(X_i \delta Y_j + \delta X_i Y_j + \delta X_i \delta Y_j \right) \mathscr{S}_Z \right). \tag{18}$$

Note that $\delta X_1 = 0$ as the receiver system simply inherits the solution to X_1 from the driver. We have tested various $(3N)$-dimensional Lorenz systems with different parameters and dimensions using the numerical solutions of Eqs. (16)–(18), whose results suggest that the error subsystem is indeed stable. An example of such results is shown in Fig. 3 for the 21-dimensional system.

4. Application in image encryption

Over the years, there have been proposed numerous encryption schemes utilizing chaotic signals to securely mask certain sensitive information in transit [7,20–23]. Many of these schemes rely on chaos synchronization to recover the 'unpredictable' chaotic signals generated from the driver's end. Although the naïve designs in early prototypes were criticized for being cryptographically weak [24–26], recent and on-going efforts that employ modern and sophisticated techniques seem to suggest the viability of these chaos-based encryption schemes [27–29].

In this section, a pixel by pixel masking of a raster image is performed to demonstrate the potential utility of self-synchronization in these generalized high-dimensional Lorenz systems. We showcase a chaos synchronization-based image
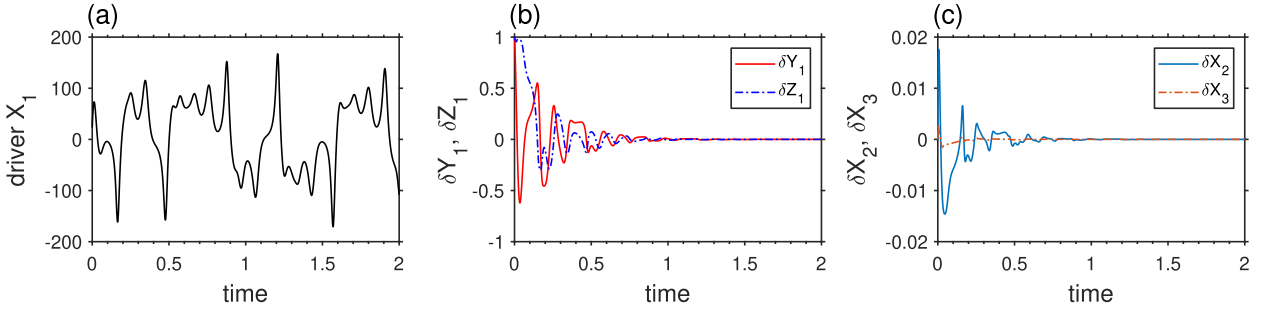
Fig. 3. (a) Time series of the numerical solutions to X_1 in the 21-dimensional Lorenz system with parameters $r = 500$, $\sigma = 50$, and $b = 8/3$ as the driver system. The responses of (b) δY_1 and δZ_1 and of (c) δX_2 and δX_3 in the error subsystem.

masking scheme using the standard test images of Baboon (Fig. 5(a)) and Barbara (Fig. 5(b)). For demonstrative purposes, here we adopt a rather intuitive approach to masking the images, namely, a simple summation-based perturbation of the color indices for each pixel. In practical implementations, the masking effectiveness of the chaotic signals generated by the $(3N)$-dimensional generalized Lorenz systems can be improved by utilizing more sophisticated encryption methods including the bitwise exclusive-or operator [30–33].

Suppose a raster image consists of ordered pixels $\mathscr{P}$, each containing three numbers that represent red (R), green (G), and blue (B). Let $(R, G, B)_i \in \mathscr{P}$ be the 3-tuple representing the ith pixel. Define a masking function m from the original pixels $\mathscr{P}$ to the masked pixels $\widetilde{\mathscr{P}}$ such that for each i,

$$m : (R, G, B)_i \mapsto (R, G, B)_i + \alpha \sum_{k=1}^{l} (X_k^{(i)}, Y_k^{(i)}, Z_k^{(i)}), \tag{19}$$

where $(X_k^{(i)}, Y_k^{(i)}, Z_k^{(i)})$ is the solution of the driver system for the kth variable set at time step i. Clearly, convergence to chaos must occur prior to using the solution to mask an image. While the convergence time varies depending on the dimension of the system and the parameter values being used [18], we found that $t \geq 50$ is a long enough spin-up time, given the parameter values used in this study. As can be seen in Fig. 1, synchronization also appears to occur fairly quickly even for systems with very high dimensions. Numerical solutions over $t \in [50, 250]$ with $\Delta t = 10^{-4}$ provide a sufficiently large number of time steps for covering test images with the resolution of 512×512. Here, $l \leq N$ stands for *level*, which is the number of (X_k, Y_k, Z_k) variable sets being used to perturb, if the amplitudes of chaotic signals are relatively small, or to envelop, if the amplitudes are much greater than the color signals, the original image, and α is an amplification factor referred to as the *intensity* of chaotic masking. Once $\widetilde{\mathscr{P}}$ is received along with the solution to X_1 by the receiver system, the original pixels $\mathscr{P}$ can then be recovered using the solutions obtained from the synchronized receiver system. The driver's initial condition does not need to be known since the receiver system under self-synchronization should be able to recover the rest of the driver's solutions regardless of the initial condition. Note that the driver sending the solutions for X_1 to the receiver in the context of the three-dimensional Lorenz system gives away 1/3 of the entire information needed to decode the encryption. With higher-dimensional systems that still only require the transmission of X_1 for self-synchronization, this fraction corresponding to the amount of information given-away gets substantially reduced. From this perspective, using high-dimensional Lorenz systems for encryption purposes has an added benefit of enhanced security.

Note that, here, an image-covering scheme of the simplest kind is chosen in order to focus on demonstrating the utility of high-dimensional Lorenz systems in image encryption, rather than one particular image encryption scheme itself. Nonetheless, there still remain several issues with the vanilla scheme using (19) which can make rendering of $\widetilde{\mathscr{P}}$ into a masked image less effective even for the demonstrative purposes. The first issue stems from the fact that unlike X_k or Y_k, which are symmetric with respect to the transformation $(X, Y) \mapsto (-X, -Y)$ [18], the fluctuating Z_k values tend to remain above 0, meaning that the blue color at the receiving end of the chaotic signal from Z will continue to intensify. A direct application of the scheme following (19) will, therefore, result in oversaturation of the blue color. This by itself is not an issue if the delivery of the masked information is done using the signal $\widetilde{\mathscr{P}}$, but it can result in an over-representation of the blue color in the rendered images. To compensate for this and other potential imbalances, a calibration process is adopted as follows. For any variable V_k, the calibrated $\hat{V}_k$ is given by

$$\hat{V}_k = V_k - \frac{1}{2} \left(\max_i V_k^{(i)} + \min_i V_k^{(i)} \right), \tag{20}$$

which is meant to simply pull down the average to 0. The second and related issue is that while chaotic signals of large amplitudes can effectively hide (or envelop) the image signal, when such an image is rendered into a masked image with the color scale ranging from 0 to 255, much information is lost from the masked signals, making it ambiguous whether the improved masking using a high-dimensional Lorenz system is due to the enhanced security from having additional chaotic layers or simply a result of under- or oversaturation. Thus, for the masked images in Fig. 4, the calibrated chaotic signals
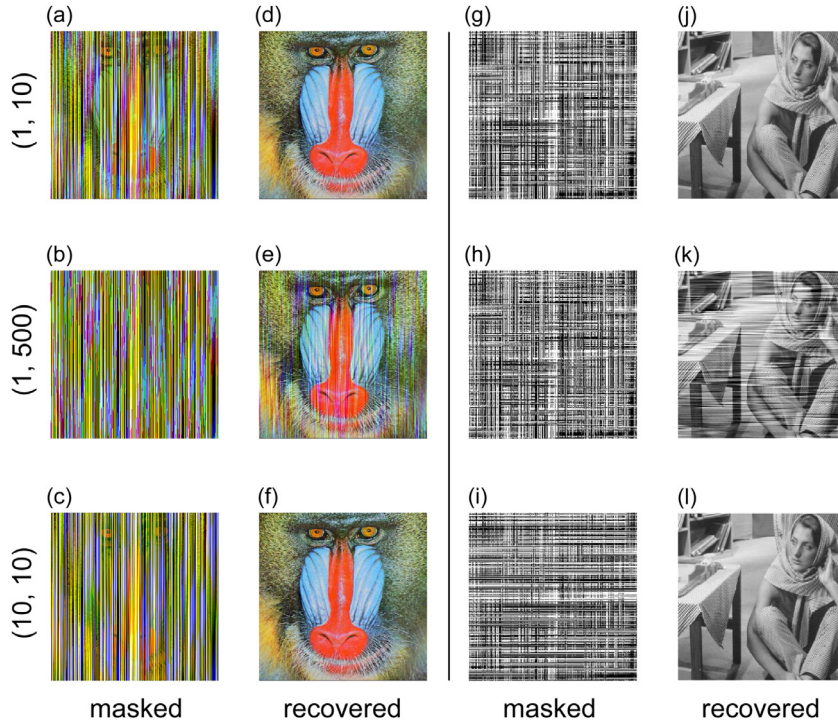
Fig. 4. Masked image of Baboon using chaotic signals from the 30-dimensional driver system with parameters $r = 500$, $\sigma = 50$, and $b = 8/3$ under (a) level 1 and intensity 10, (b) level 1 and intensity 500, and (c) level 10 and intensity 10. Recovered image of Baboon using the self-synchronizing receiver's solutions under (d) level 1 and intensity 10, (e) level 1 and intensity 500, and (f) level 10 and intensity 10. (g)–(i) and (j)–(l) are the same as (a)–(c) and (d)–(f), respectively, except the black-and-white image of Barbara is used.

have undergone normalization via

$$\sum_{k=1}^{l} \hat{V}_k^{(i)} \mapsto \frac{255 \sum_{k=1}^{l} \hat{V}_k^{(i)}}{255 + \max_i \left\{ \sum_{k=1}^{l} \hat{V}_k^{(i)} \right\} - \min_i \left\{ \sum_{k=1}^{l} \hat{V}_k^{(i)} \right\}}, \tag{21}$$

where $V_k = X_k$, Y_k, or Z_k for all k.

Fig. 4(a)–(c) are the masked images of Baboon using (level, intensity) $= (l, \alpha) = (1, 10)$, (level, intensity) $= (1, 500)$, and (level, intensity) $= (10, 10)$, respectively. Setting $l = 1$ is effectively equivalent to using the three-dimensional system, and since $l \leq N$, using a higher dimension of the generalized system unlocks higher levels to become available. Fig. 4(d)–(f) are the recovered images from the masked images in Fig. 4(a)–(c), respectively. Note that in this simple masking scheme the pixels to be perturbed are sequentially ordered from the top to bottom, thus creating the columnar patterns in the masked images. In practical use, one can utilize a more sophisticated algorithm to redistribute sequential ordering of the pixels, which will make the masking patterns less obvious. As for black-and-white images such as that of Barbara in Fig. 5(b), the masking scheme following (19) is not directly applicable since each pixel is represented by a single number indicating its grayscale rather than by an rgb 3-tuple. In this case, we have opted to utilize the chaotic solutions for the X variables to mask the pixels ordered in the columnar direction, as is done for Fig. 4(a)–(c), and use the chaotic solutions for the Y variables to mask the image again in the horizontal direction, creating a kind of a mesh in the resulting masked image of Barbara shown in Fig. 4(g)–(i). Having two chaotic signals criss-cross in both the horizontal and vertical directions for Barbara instead of in just one direction as is done for Baboon appears to markedly improve the effectiveness of masking, but this could be due to other skewing factors such as the particular image being more susceptible to masking.

There exist many different methods for evaluating the effectiveness of chaos-based image masking schemes, most of which focus on randomness of the masked image [33]. One such method is to compute the correlation coefficients between adjacent pixels, sweeping across the image horizontally (comparing the columns) or vertically (comparing the rows), or diagonally [34]. In this method, an unaltered image is known to yield the correlation coefficients fairly close to 1, and the closer the correlation coefficients are to 0, the more random the altered image is determined to be. While our masking scheme does not exactly result in random noise, such a method can still be utilized to quantitatively compare the relative performance of the scheme under different settings. The average correlation coefficients amongst the adjacent columns (across horizontal) and the diagonals in the original and altered images from Fig. 4 are summarized in Table 1. The original images yield the average correlation coefficients > 0.8 both horizontally and diagonally. The masked images of Baboon have the average correlation coefficients between the adjacent columns below 0.2. The average correlation coefficients between
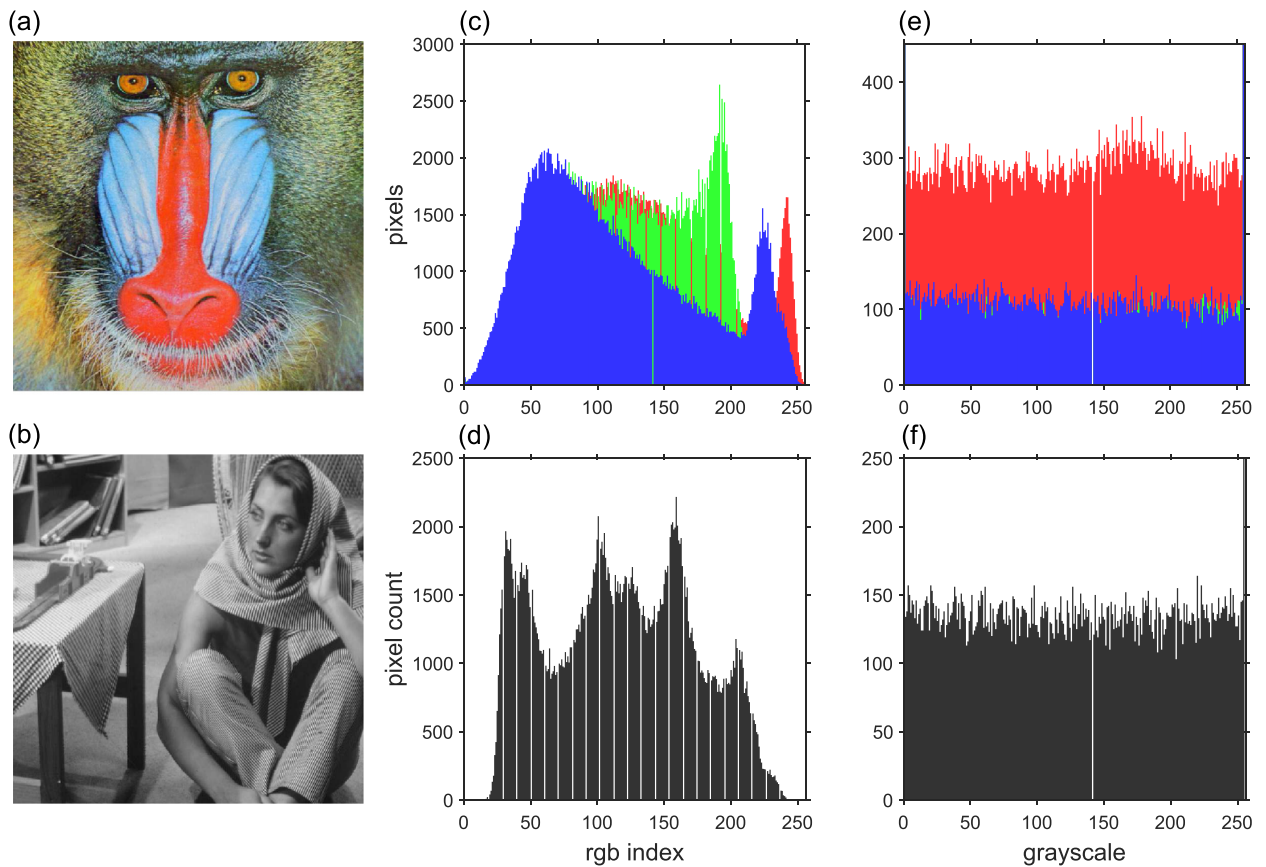
Fig. 5. Original image of (a) Baboon and (b) Barbara. Histogram showing the pixel distribution in terms of the rgb or grayscale intensity in the original image of (c) Baboon and (d) Barbara. Histogram showing the pixel distribution in terms of the rgb or grayscale intensity in the masked image of (e) Baboon and (f) Barbara, corresponding to Fig. 4(c) and (i), respectively.

Table 1

Correlation coefficients against the original image (Fig. 5(a) and (b)) and the average correlation coefficients between adjacent columns (horizontal) and diagonals for each original and altered image in Fig. 4. The displayed numbers for the color image, Baboon, are averages of three correlation coefficients from the red, green, and blue color indices.

Image/status	Correlation against	Correlation between adjacent pixels	
(level, intensity)	original image	Horizontal	Diagonal
Baboon/original	-	0.8479	0.8116
Baboon/masked			
(1, 10)	0.1811	0.1401	0.1607
(1, 500)	0.0130	0.1114	0.1441
(10, 10)	0.1295	0.1724	0.2294
Baboon/recovered			
(1, 10)	0.9998	0.8476	0.8113
(1, 500)	0.7848	0.5552	0.5502
(10, 10)	0.9998	0.8476	0.8113
Barbara/original	-	0.8789	0.9378
Barbara/masked			
(1, 10)	0.1233	0.6382	0.0550
(1, 500)	0.0085	0.6342	0.0484
(10, 10)	0.1028	0.8395	0.1069
Barbara/recovered			
(1, 10)	0.9998	0.8790	0.9373
(1, 500)	0.7273	0.9405	0.4018
(10, 10)	0.9998	0.8789	0.9374

the diagonals in the masked Barbara images are $\lesssim 0.1$. Note that because in the Baboon image the masking is applied to the pixels that are ordered in the vertical direction, the correlation coefficients between the adjacent rows are necessarily fairly high, and for this reason these computations are excluded from Table 1. Likewise, only the correlation coefficients between the diagonals yield meaningful results concerning the masked images of Barbara in Fig. 4(g)–(i), in which the masking is applied to the pixels upon ordering them both vertically and horizontally. The relatively high average correlation coefficients between the adjacent columns in the masked Barbara images can be attributed to this reason.

As a direct measure of masking-effectiveness, Table 1 also includes the correlation coefficients between all pixels of the masked and original images. The correlation coefficients between the masked and original images generally fall below 0.15 except for the low level–low intensity case for Baboon. The correlation coefficients are exceptionally low for the high-intensity cases, and the masked images for the high-level cases generally show weaker correlations with the original image compared to the corresponding low level–low intensity cases. The masking performances of Fig. 4(c) and (i) are further examined through the histograms showing their color or grayscale distributions among the pixels before (Fig. 5(c) and (d)) and after (Fig. 5(e) and (f)) masking. It is known that the more uniform the distribution is, the more robust the image encryption can be, providing some protection against statistical attacks [32]. The histograms for both the Baboon and Barbara images masked with level 10 and intensity 10 can be said to exhibit distributions that are more uniform compared to the original images.

In Fig. 4, it is shown that there are two ways to improve the security of chaotic masking; namely, raising the level l and raising the intensity α. The effectiveness of masking appears to be fairly poor in the low level–low intensity case in Fig. 4(a). Raising the intensity improves the masking effectiveness as can be readily seen in Fig. 4(b) but at the expense of poor quality in the recovered image as apparent from Fig. 4(e) and (k), corresponding to the correlation coefficients of 0.7848 and 0.7273 against the original, respectively. On the other hand, raising the level instead of the intensity, as in Fig. 4(c) and (f) or Fig. 4(i) and (l), improves the security of masking while, at the same time, being able to preserve the recovered image quality comparable to using the low level–low intensity case in Fig. 4(d) and (j), with the correlation coefficient of 0.9998 against the original in both cases.

The deterioration of image quality visible in Fig. 4(e) and (k) is caused by the seemingly unavoidable yet minuscule differences between the driver's and receiver's solutions, which becomes amplified by the factor α. The noise persists even after the two systems are effectively in synchrony. If a mathematical proof of exact self-synchronization in the generalized $(3N)$-dimensional systems is found, for example by finding a Lyapunov function [19] or by taking a more general approach [35,36], then we are assured that the persistent noise is purely numerical. In this way, finding the proof of self-synchronization in these $(3N)$- and $(3N + 2)$-dimensional generalizations of the Lorenz system takes on an additional layer of practicality.

5. Beyond self-synchronization

Experimenting further by assigning systems with different dimensions as the driver and the receiver while still transmitting only X_1 from the driver to the receiver, we stumbled onto a curious phenomenon that goes beyond self-synchronization. Note that even when the driver and receiver systems are different, the two systems are still related in our set-up. In the $(3N)$- and $(3N + 2)$-dimensional generalizations of [17], any system with a higher dimension essentially contains all systems with lower dimensions. For this reason, how different the driver and receiver systems are from each other can be quantified by the dimensional difference between the two. The question is whether there is any hint of synchronization left when the two coupled systems have different dimensions, and if so, whether that depends on how close or far apart the two systems are, which in turn can be measured by their dimensional difference.

Fig. 6(a) and (b) show the difference trajectories for the cases corresponding to self-synchronization. The latter portions of the trajectories (solid with changing colors) are barely visible in Fig. 6(a) and (b) because the differences between the driver's and receiver's solutions to Y_1 and Z_1 quickly close in on 0. In contrast, when the driver and receiver systems have different dimensions as in Fig. 6(c) and (d), the difference trajectories do not quite converge to 0, although their magnitudes seem to be bounded, fluctuating with smaller amplitudes after some time. This suggests that although there is no complete synchronization comparable to self-synchronization when the two systems have different dimensions, the receiver system does get influenced by the driver system to some extent and in the direction following the driver system's solution. In other words, such couplings still retain some traces of synchronization.

To quantify how much out of sync they become, the rmsd in the numerical solutions between the driver and receiver systems are computed. Each marker in Fig. 7 corresponds to a particular dimension and parameter choice. Here, the (r, σ) parameter pairs are chosen from $r \in \{500, 520, 550, 575, 600\}$ and $\sigma \in \{50, 51, 52\}$ with which the $(3N)$-dimensional systems up to dimension 30 all have chaotic solutions [17]. The rmsd are computed over $t \in [4.5, 10]$. The initial conditions $X_1 = 1$ and $X_1 = 100$ are used for the driver and receiver systems, respectively, with all other variables set to 0 initially. Surprisingly, Fig. 7 shows a positive correlation between the dimensional difference and how closely in sync the two systems are. This means that the general direction of how well the two systems synchronize is in agreement with achieving perfect or near-perfect synchrony when the two systems are identical. This phenomenon is also readily seen in the trajectories. Fig. 8 shows that the further apart the dimension of the receiver system is from that of the driver system, the more dissimilar their trajectories tend to become, resulting in greater rmsd.

To see if there are differences in the patterns with which the rmsd and dimension are correlated, the correlation coefficients for various groupings of scatters are computed and summarized in Table 2. Overall, the correlation coefficients are
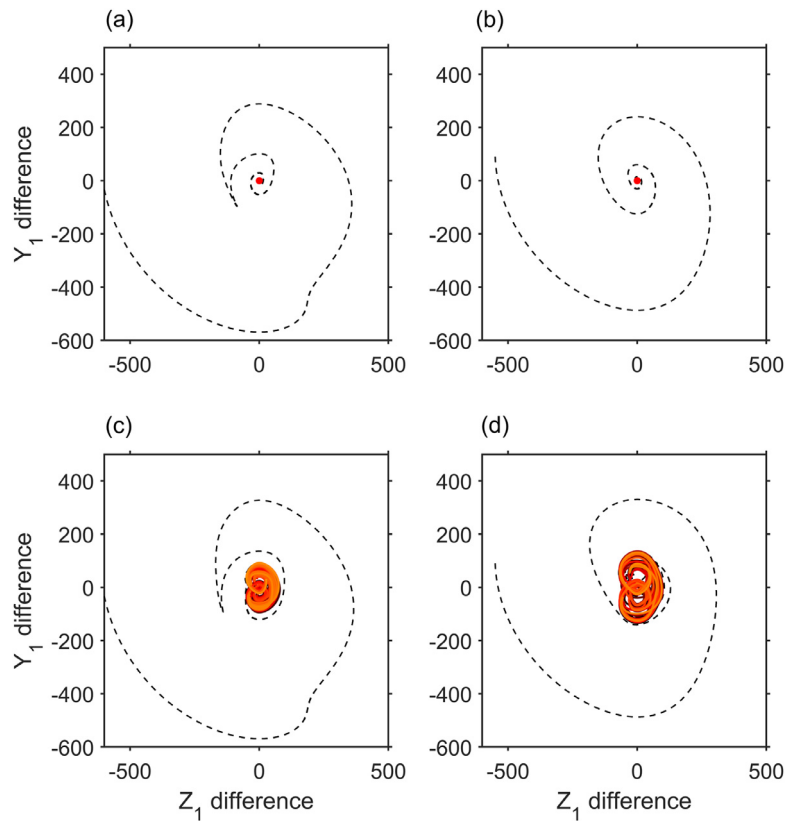
Fig. 6. Trajectories of the difference in the solutions for Y_1 and Z_1 between the driver and the receiver systems whose dimensions are given by (a) 24 and 24, (b) 30 and 30, (c) 24 and 18, and (d) 30 and 18, respectively. The black dashed curves indicate the first 1/3 of the difference trajectories and solid lines in different colors are used for the latter portions of the trajectories. For (a) and (b), the end point of the trajectories are marked by red dots.
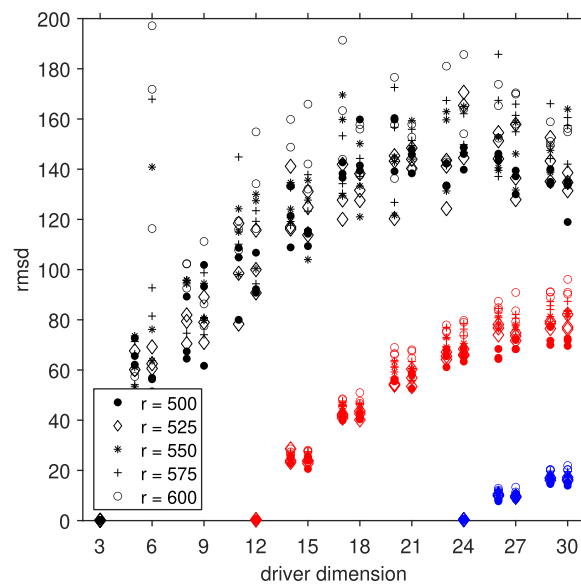
Fig. 7. Root-mean-square difference between the driver's and receiver's solutions as a function of driver's dimension with the receiver system dimension set to 3 (black), 12 (red), and 24 (blue). Different markers indicate the associated r values.
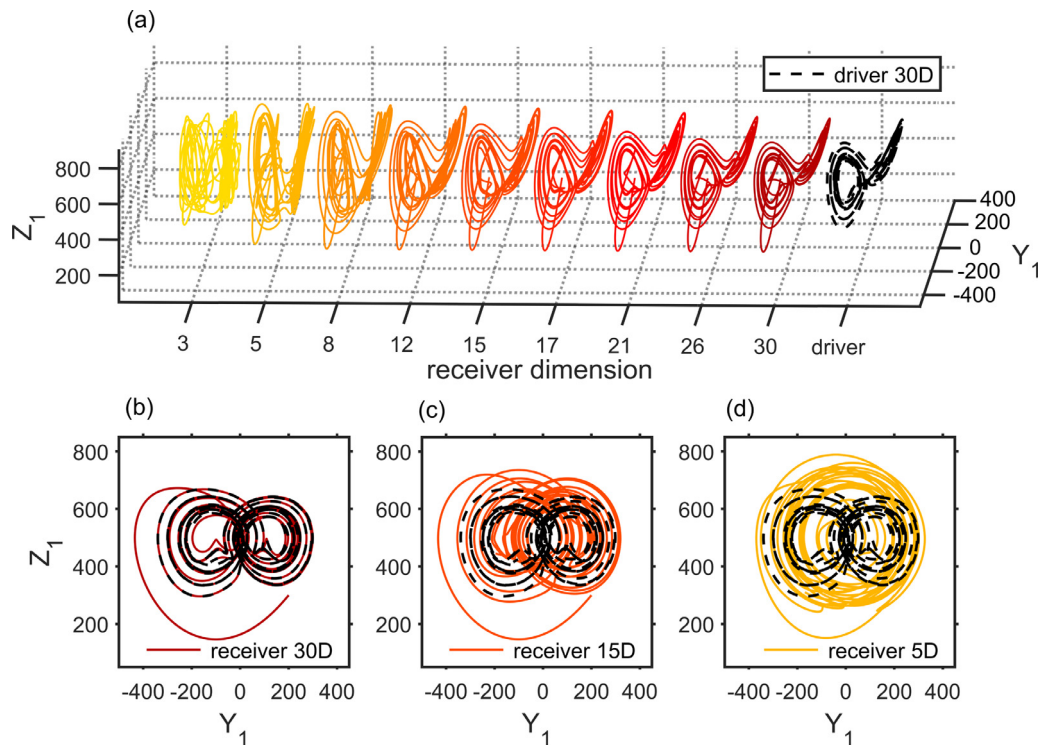
Fig. 8. Trajectories of the receiver's solutions in the systems of dimensions (a) 3, 5, 8, 12, 15, 17, 21, 26, and 30 synchronizing with the driver system of dimension 30, projected on the $Y_1 - Z_1$ plane. The parameters are given by $r = 500$, $\sigma = 50$, and $b = 8/3$. The $Y_1 - Z_1$ projection of the driver's solution trajectory (black, dashed) superposed on top of the receiver's solution trajectory (other colors, solid) with the receiver system's dimension given by (b) 30, (c) 15, and (d) 5. The driver's initial condition at $t = 0$ is given by $(X_1, Y_1, Z_1, \ldots) = (1, 0, 0, \ldots)$. The receiver's initial condition at $t = 1$ when the coupling starts is the same as the driver's except $Y_1 = 200$ and $Z_1 = 300$ in the receiver system.

Table 2
Average correlation coefficients corresponding to the relationship between the rmsd (between the 30-dimensional driver system's solutions and the receiver solutions) and the dimensional difference between the driver and receiver systems observed in Fig. 7, classified based on the r values and the receiver system's dimension.

	r value					Receiver dimension		
	500	525	550	575	600	3	12	24
Correlation	0.9083	0.9240	0.8983	0.9041	0.8666	0.7883	0.9513	0.9611

fairly close to 1 and are greater if the receiver system's dimension is higher, which can also be seen in Fig. 7 with the blue markers being more tightly aligned with one another compared to the red or black markers. This is expected since assigning a high-dimensional system to the receiver brings the receiver system closer to the 30-dimensional system assigned to the driver, leaving very little wiggle room for the receiver system to act on its own independently of the driver's solutions. As for the groups of scatters classified based on the r values, the correlation coefficients range from 0.8666 to 0.9240, but there are no signs indicating their dependence on parameter values in any particular direction.

The negative relationship between the level of synchronization and the dimensional difference between the driver and receiver systems is also apparent in Fig. 9, which shows the maximum differences between the driver's and receiver's solutions corresponding to the dimensions of the two systems, computed with $r = 500$ and $\sigma = 50$. As expected, the maximum differences are significantly lower along the diagonal of Fig. 9 and its vicinity, which is indicative of synchronization when the two systems have equal or nearly equal dimensions. Observe also that the maximum differences tend to be slightly smaller when the driver's dimension is greater than the receiver's dimension compared to the other way around. This is expected because our coupling set-up is unidirectional from the driver to receiver systems. If the driver's dimension is higher than the receiver's dimension, then at least some of the extraneous information from the driver's other variables is transmitted to the receiver system through the coupling. On the other hand, if the receiver system's dimension is higher than that of the driver system, then the extraneous variables are on the receiver's side. In that case, the extra noise produced from the interactions involving these additional variables in the receiver system is not fed back into the driver system, creating further discrepancies between the driver's and receiver's solutions.
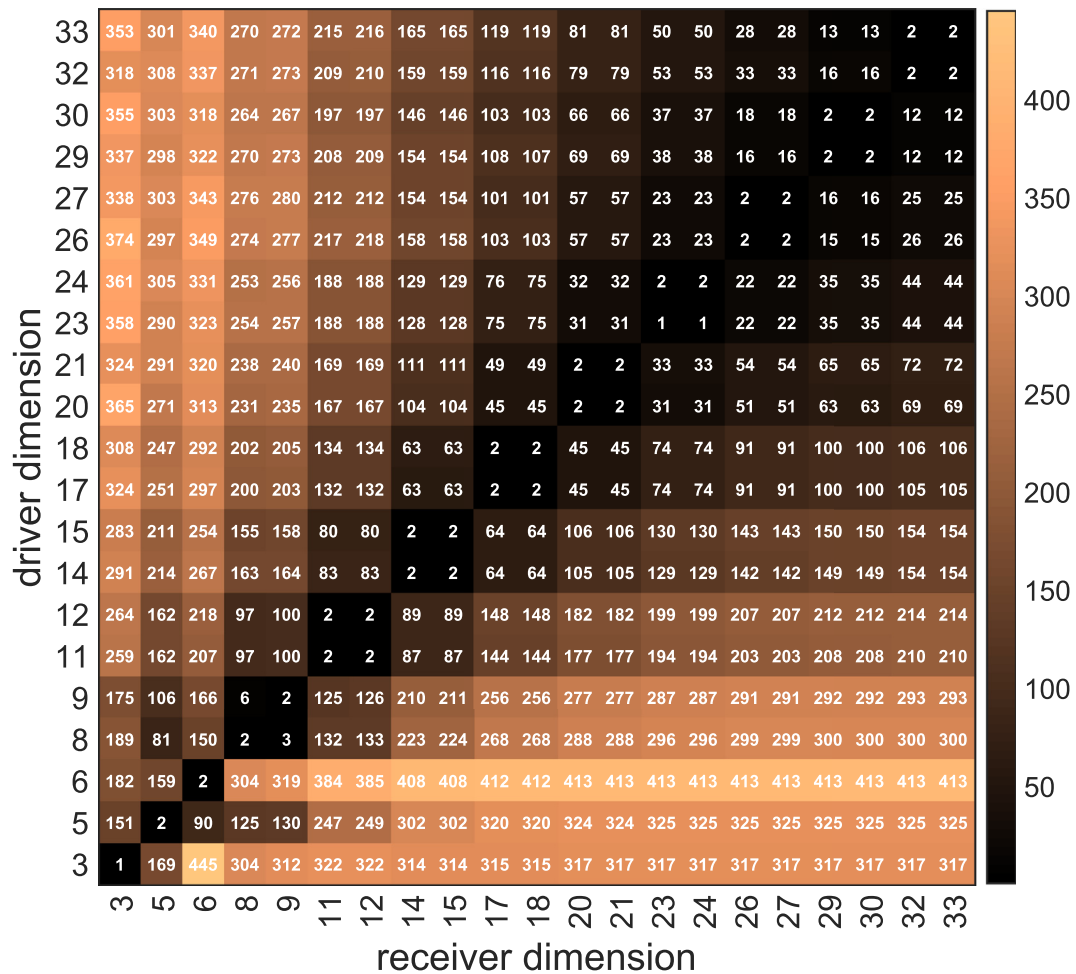
driver dimension \ receiver dimension	3	5	6	8	9	11	12	14	15	17	18	20	21	23	24	26	27	29	30	32	33
33	353	301	340	270	272	215	216	165	165	119	119	81	81	50	50	28	28	13	13	2	2
32	318	308	337	271	273	209	210	159	159	116	116	79	79	53	53	33	33	16	16	2	2
30	355	303	318	264	267	197	197	146	146	103	103	66	66	37	37	18	18	2	2	12	12
29	337	298	322	270	273	208	209	154	154	108	107	69	69	38	38	16	16	2	2	12	12
27	338	303	343	276	280	212	212	154	154	101	101	57	57	23	23	2	2	16	16	25	25
26	374	297	349	274	277	217	218	158	158	103	103	57	57	23	23	2	2	15	15	26	26
24	361	305	331	253	256	188	188	129	129	76	75	32	32	2	2	22	22	35	35	44	44
23	358	290	323	254	257	188	188	128	128	75	75	31	31	1	1	22	22	35	35	44	44
21	324	291	320	238	240	169	169	111	111	49	49	2	2	33	33	54	54	65	65	72	72
20	365	271	313	231	235	167	167	104	104	45	45	2	2	31	31	51	51	63	63	69	69
18	308	247	292	202	205	134	134	63	63	2	2	45	45	74	74	91	91	100	100	106	106
17	324	251	297	200	203	132	132	63	63	2	2	45	45	74	74	91	91	100	100	105	105
15	283	211	254	155	158	80	80	2	2	64	64	106	106	130	130	143	143	150	150	154	154
14	291	214	267	163	164	83	83	2	2	64	64	105	105	129	129	142	142	149	149	154	154
12	264	162	218	97	100	2	2	89	89	148	148	182	182	199	199	207	207	212	212	214	214
11	259	162	207	97	100	2	2	87	87	144	144	177	177	194	194	203	203	208	208	210	210
9	175	106	166	6	2	125	126	210	211	256	256	277	277	287	287	291	291	292	292	293	293
8	189	81	150	2	3	132	133	223	224	268	268	288	288	296	296	299	299	300	300	300	300
6	182	159	2	304	319	384	385	408	408	412	412	413	413	413	413	413	413	413	413	413	413
5	151	2	90	125	130	247	249	302	302	320	320	324	324	325	325	325	325	325	325	325	325
3	1	169	445	304	312	322	322	314	314	315	315	317	317	317	317	317	317	317	317	317	317

Fig. 9. Maximum differences in Z_1 between the driver and receiver systems with $r = 500$ and $\sigma = 50$ over $t \in [60, 70]$ in which the initial condition for the driver systems is given by $(X_1, Y_1, Z_1, \ldots) = (1, 0, 0, \ldots)$ at $t = 0$ and the initial condition for the receiver systems is given by $(X_1, Y_1, Z_1, \ldots) = (100, 0, 0, \ldots)$ at $t = 50$ as the coupling starts. The numbers inside the cells are the maximum difference values rounded to the nearest integer.

6. Summary and discussion

The numerical experiments strongly indicate that self-synchronization occurs in the $(3N)$- and $(3N + 2)$-dimensional generalizations of the Lorenz system in the same way that the three-dimensional Lorenz system self-synchronizes. Such a property may find its uses in applications such as image encryption if combined with sufficiently sophisticated algorithms. Analyses of numerical results have also led to the identification of a broader pattern between the dimensional difference and the degree of generalized synchronization when the driver and receiver systems are assigned Lorenz systems with two different dimensions. It is particularly interesting that such a pattern appears to be in agreement with the general direction toward self-synchronization and thus has a potential to be part of some generalizing principles linking self-synchronization and generalized synchronization in these systems.

Despite the encouraging results from the numerical experiments, whether precise self-synchronization in the mathematical sense truly occurs in these generalized systems will remain as an open question until a rigorous proof is found. Further investigation of the numerical results hinting at a more general relationship between dimension and synchrony may also lead to a proof of self-synchronization in these systems as a special case when the two systems are assigned the same dimension.

Synchronization between two systems with different dimensions can also provide an interesting insight relevant to modeling of natural phenomena. It is possible that certain nonlinear systems in nature, such as the atmosphere, have higher dimensions than the approximate models currently in use, partly because of the limitations in grid resolution and also because of our limited knowledge of the real system. In any case, an accurate simulation of the reality by a model can be thought of as the synchronization between a higher-dimensional driver system and a lower-dimensional receiver system with observations functioning as the information transfer from the driver to the receiver. From this point of view, the syn-

chronizing features explored in this study can make these generalized systems suitable for use in testing data assimilation schemes. Data assimilation is currently undergoing rapid progression in the field of atmospheric science for the purpose of optimally combining observation data with model outputs [37]. We plan on further pursuing such applications of these generalized Lorenz systems in a future study.

Declaration of Competing Interest

The authors declare that they do not have any financial or nonfinancial conflict of interests

CRediT authorship contribution statement

Sungju Moon: Conceptualization, Methodology, Software, Formal analysis, Investigation, Writing - original draft, Writing - review & editing, Visualization. **Jong-Jin Baik:** Conceptualization, Supervision, Investigation, Writing - review & editing, Project administration, Funding acquisition. **Jaemyeong Mango Seo:** Methodology, Validation, Investigation, Writing - review & editing, Visualization.

Acknowledgments

References

[1] Lorenz EN. Deterministic nonperiodic flow. J Atmos Sci 1963;20:130–41.
[2] Afraimovich VS, Verichev NN. Stochastic synchronization of oscillation in dissipative systems. Radiophys Quantum Electron 1986;29:795–803.
[3] Pecora LM, Carroll TL. Synchronization in chaotic systems. Phys Rev Lett 1990;64:821–4.
[4] Blasius B, Huppert A, Stone L. Complex dynamics and phase synchronization in spatially extended ecological systems. Nature 1999;399:354–9.
[5] Tsonis AA, Swanson K, Kravtsov S. A new dynamical mechanism for major climate shifts. Geophys Res Lett 2007;34:L13705.
[6] Yang S-C, Baker D, Li H, Cordes K, Huff M, Nagpal G, et al. Data assimilation as synchronization of truth and model: experiments with the three-variable Lorenz system. J Atmos Sci 2006;63:2340–54.
[7] Cuomo KM, Oppenheim AV. Circuit implementation of synchronized chaos with applications to communication. Phys Rev Lett 1993;71:65–8.
[8] Peng JH, Ding EJ, Ding M, Yang W. Synchronizing hyperchaos with a scalar transmitted signal. Phys Rev E 1997;55:297–9.
[9] Tamaševičius A, Čenys A. Synchronizing hyperchaos with a single variable. Phys Rev Lett 1996;76:904–7.
[10] Musielak ZE, Musielak DE. High-dimensional chaos in dissipative and driven dynamical systems. Int J Bifurc Chaos 2009;19:2823–69.
[11] Shen B-W. Nonlinear feedback in a five-dimensional Lorenz model. J Atmos Sci 2014;71:1701–23.
[12] Shen B-W. Nonlinear feedback in a six-dimensional Lorenz model: impact of an additional heating term. Nonlinear Process Geophys 2015;22:749–64.
[13] Park J, Han B-S, Lee H, Jeon Y-L, Baik J-J. Stability and periodicity of high-order Lorenz-Stenflo equations. Phys Scr 2016;91:065202.
[14] Felicio CC, Rech PC. On the dynamics of five- and six-dimensional Lorenz models. J Phys Commun 2018;2:025028.
[15] Rech PC. On the dynamics of a high-order Lorenz-Stenflo system. Phys Scr 2016;91:125201.
[16] Rech PC. On the dynamics in parameter planes of the Lorenz-Stenflo system. Phys Scr 2015;90:115201.
[17] Moon S, Seo JM, Baik J-J. High-dimensional generalizations of the Lorenz system and implications for predictability. Phys Scr 2020;95:085209.
[18] Moon S, Han B-S, Park J, Seo JM, Baik J-J. Periodicity and chaos of high-order Lorenz systems. Int J Bifurc Chaos 2017;27:1750176.
[19] He R, Vaidya PG. Analysis and synthesis of synchronous periodic and chaotic systems. Phys Rev A 1992;46:7387–92.
[20] Ogorzałek MJ. Taming chaos – Part I: synchronization. IEEE Trans Circuits Syst I 1993;40:693–9.
[21] Kocarev L, Parlitz U. General approach for chaotic synchronization with applications to communication. Phys Rev Lett 1995;74:5028–31.
[22] Alvarez G, Li S. Some basic cryptographic requirements for chaos-based cryptosystems. Int J Bifurc Chaos 2006;16:2129–51.
[23] Pisarchik AN, Flores-Carmona NJ, Carpio-Valadez M. Encryption and decryption of images with chaotic map lattices. Chaos 2006;16:033118.
[24] Pérez G, Cerdeira HA. Extracting messages masked by chaos. Phys Rev Lett 1995;74:1970–3.
[25] Zhou H, Ling X-T. Problems with the chaotic inverse system encryption approach. IEEE Trans Circuits Syst I 1997;44:268–71.
[26] Sundar S, Minai AA. Synchronization of randomly multiplexed chaotic systems with application to communication. Phys Rev Lett 2000;85:5456–9.
[27] Argyris A, Syvridis D, Larger L, Annovazzi-Lodi V, Colet P, Fischer I, et al. Chaos-based communications at high bit rates using commercial fibre-optic links. Nature 2005;438:343–6.
[28] Kinzel W, Englert A, Kanter I. On chaos synchronization and secure communication. Philos Trans R Soc A 2010;368:379–89.
[29] Keuninckx L, Soriano MC, Fischer I, Mirasso CR, Nguimdo RM, Van der Sande G. Encryption key distribution via chaos synchronization. Sci Rep 2017;7:43428.
[30] Xu Y, Wang H, Li Y, Pei B. Image encryption based on synchronization of fractal chaotic systems. Commun Nonlinear Sci Numer Simul 2014;19:3735–44.
[31] Hammami S. State feedback-based secure image cryptosystem using hyperchaotic synchronization. ISA Trans 2015;54:52–9.
[32] Luo Y, Du M, Liu J. A symmetrical image encryption scheme in wavelet and time domain. Commun Nonlinear Sci Numer Simul 2015;20:447–60.
[33] Nepomuceno EG, Nardo LG, Arias-Garcia J, Butusov DN, Tutueva A. Image encryption based on the pseudo-orbits from 1D chaotic map. Chaos 2019;29:061101.
[34] Diaconu A-V, Dascalescu AC. Correlation distribution of adjacent pixels randomness test for image encryption. Proc Rom Acad Ser A 2017;18:351–60.
[35] Blekhman II, Fradkov AL, Nijmeijer H, Pogromsky AY. On self-synchronization and controlled synchronization. Syst Control Lett 1997;31:299–305.
[36] Blekhman II, Fradkov AL, Tomchina OP, Bogdanov DE. Self-synchronization and controlled synchronization: general definition and example design. Math Comput Simul 2002;58:367–84.
[37] Kalnay E. Atmospheric modeling, data assimilation and predictability. 1st ed. New York: Cambridge University Press; 2003.